Molecular Therapy
Methods & Clinical Development
Original Article

Large-Scale Generation and Characterization of Homogeneous Populations of Migratory Cortical Interneurons from Human Pluripotent Stem Cells

Peiyan Ni,[1,2,3] Haneul Noh,[2,3] Zhicheng Shao,[3] Qian Zhu,[2] Youxin Guan,[2] Joshua J. Park,[2] Fatima Arif,[2] James M. Park,[2] Chiderah Abani,[2] Cameron Beaudreault,[2] Joy S. Park,[2] Elizabeth Berry,[2] Alexander Moghadam,[2] Patric Stanton,[2] John N. Hutchinson,[4] Bill Andrews,[5] Clare Faux,[5] John Parnevelas,[5] Leonard M. Eisenberg,[6] Kyungjoon Park,[3] Vadim Y. Bolshakov,[3] and Sangmi Chung[2,3]

[1]Psychiatric Laboratory and Mental Health Center, The State Key Laboratory of Biotherapy, West China Hospital of Sichuan University, Chengdu 610041, China; [2]Department of Cell Biology and Anatomy, New York Medical College, Valhalla, NY 10595, USA; [3]Department of Psychiatry, McLean Hospital and Harvard Medical School, Belmont, MA 02478, USA; [4]Department of Biostatistics, Harvard Chan School of Public Health, Boston, MA 02115, USA; [5]Department of Cell and Developmental Biology, University College London, London WC1 6BT, UK; [6]Departments of Physiology and Medicine, New York Medical College and Westchester Medical Center Stem Cell Laboratory, New York Medical College, Valhalla, NY 10595, USA

During development, cortical interneurons (cINs) are generated from the ventral telencephalon, robustly migrate to the dorsal telencephalon, make local synaptic connections, and critically regulate brain circuitry by inhibiting other neurons. Thus, their abnormality is associated with various brain disorders. Human pluripotent stem cell (hPSC)-derived cINs can provide unlimited sources with which to study the pathogenesis mechanism of these disorders as well as provide a platform to develop novel therapeutics. By employing spinner culture, we could obtain a >10-fold higher yield of cIN progenitors compared to conventional culture without affecting their phenotype. Generated cIN spheres can be maintained feeder-free up to 10 months and are optimized for passaging and cryopreservation. In addition, we identified a combination of chemicals that synchronously matures generated progenitors into $SOX6^{+}KI67^{-}$ migratory cINs and extensively characterized their maturation in terms of metabolism, migration, arborization, and electrophysiology. When transplanted into mouse brains, chemically matured migratory cINs generated grafts that efficiently disperse and integrate into the host circuitry without uncontrolled growth, making them an optimal cell population for cell therapy. Efficient large-scale generation of homogeneous migratory cINs without the need of feeder cells will play a critical role in the full realization of hPSC-derived cINs for development of novel therapeutics.

INTRODUCTION

Cortical interneurons (cINs), especially those subtypes that express parvalbumin (PV), and somatostatin (SST), are derived from the medial ganglionic eminence (MGE) in the subpallium during early development. They migrate all the way to the dorsal telencephalon, where they make local synaptic connections with excitatory glutamatergic neurons and critically regulate local brain circuitry by releasing the inhibitory neurotransmitter γ-aminobutyric acid (GABA).[1,2] Compromised function of these cINs is associated with various brain disorders, such as schizophrenia, autism, and epilepsy.[3,4] Furthering our understanding of the cIN-associated disease pathogenesis mechanism depends on securing relevant tissue sources for analysis. Obtaining relevant brain tissues during the pathogenesis process was once extremely challenging with the exception of end-stage postmortem tissues or rare resected patient brain tissues. However, it is now possible to generate disease-relevant tissues in unlimited quantity with exactly the same genetic makeup as the patient with the development of induced pluripotent stem cell (iPSC) technology,[5] as long as efficient ways to generate a homogeneous population of specific progenies can be identified.

Not only do they provide clues to normal and abnormal developmental process in health and disease, but human PSC-derived neurons can also serve as a source of cells for cell-replacement therapy, allowing treatment of brain disorders for patients without other effective treatment options.[6–12] In particular, iPSC-derived neuronal progenies could provide autologous cell sources for cell replacement without the need for immunosuppression or concerns over immune rejection. Cell transplantation, especially transplantation of cINs, was shown to provide improvement of symptoms in diverse preclinical models of CNS disorders such as epilepsy, Parkinson's disease, neuropathic pain, schizophrenia, and cognitive deficits.[6,13–16] Transforming these promising preclinical studies into a clinical reality critically depends on the ability to generate large quantities of homogeneous cell populations that are in the optimal stage of development for therapeutic use.

Received 2 February 2019; accepted 1 April 2019;
https://doi.org/10.1016/j.omtm.2019.04.002.

Correspondence: Sangmi Chung, Department of Cell Biology and Anatomy, New York Medical College, 15 Dana Rd., Valhalla, NY 10595, USA.
E-mail: schung8@nymc.edu

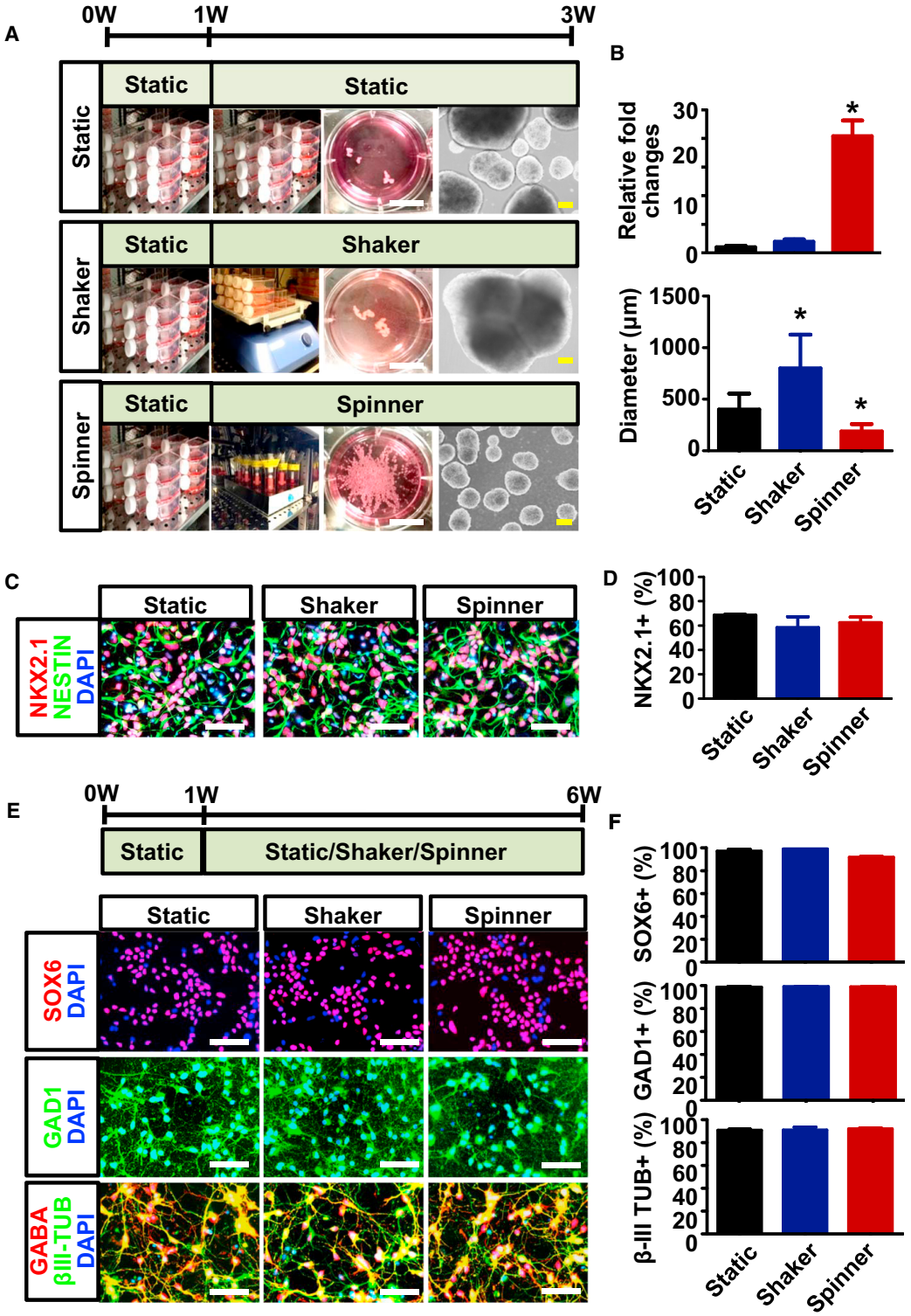

Figure 1. Optimization of Large-Scale Generation of MGE cIN Progenitors

(A) Scheme of MGE progenitor phenotype induction from hPSCs. White scale bar, 5 mm. Yellow scale bar, 200 μm. (B) Spinner culture efficiently generated H9 MGE progenitor populations in large quantities. Spheres under different culture conditions were trypsinized at the end of week 3 for cell counting. One-way ANOVA ($p < 0.001$) followed by Tukey post-hoc analysis was performed to analyze the relative changes in total cell numbers and sphere sizes (Table S3). Data are presented as mean ± SEM

(legend continued on next page)

MGE progenitors and cINs have been derived from human pluripotent stem cells (hPSCs) either by activating the developmentally relevant signaling pathways during differentiation[6,17–19] or by direct induction using exogenous expression of fate-inducing transcription factors.[20–22] However, large-scale generation of cINs that can meet the demand of translational and clinical use for disease modeling, drug screening, and/or cell therapy have not been demonstrated. Protracted maturation of human cINs requires more time in culture to achieve the proper maturation for disease modeling or cell therapy. Most of these methods involve coculture with other cell types such as astrocytes or glutamatergic neurons to support long-term maturation and maintenance *in vitro*,[17,19,20,22] yielding mixtures of cell populations with variable functional properties. This is not optimal for transcriptome analysis or cell therapy use and awaits a more homogeneous culture system that supports long-term culture. In addition, hPSC-derived neuronal progenies are usually asynchronous, composed of proliferating progenitors and postmitotic neurons at the same time (just as during normal development); such stochasticity and heterogeneity always raises the concern of unreliable assays for disease modeling[23] and graft safety for cell therapy.[24,25] Protracted maturation of the cINs themselves is a hurdle in the efficient use of cINs for various assays, raising the cost and time required before attaining a reasonable maturation status for utilization and assay. This requires the development of a method that can synchronously facilitate the maturation of cINs, preferably without genetic modifications that pose the risk of insertional mutagenesis that can compromise both disease study and cell therapy.

In this study, we addressed the major issues that are in the way of efficient application of hPSC-derived cINs to further our knowledge in disease pathogenesis and to develop novel therapeutics. We optimized spinner culture of three-dimensional (3D) cIN spheres to support the industrial-scale generation of homogeneous cIN populations. This feeder-free culture system sustained generated cINs in the long term without compromising their survival or phenotype and was optimized for passaging and cryopreservation with the incorporation of Trehalose. Moreover, we have optimized their synchronized maturation into early postmitotic migratory cINs using a cocktail of chemicals, confirming their maturation in terms of metabolism, migration, arborization, and electrophysiology. Furthermore, chemical treatment of hPSC-derived MGE cells was efficient in controlling proliferation in the grafts after transplantation into Nod Scid mouse brains and promoting migration and integration of grafted cells in the host brains. This efficient method will bring clinical translation of cIN cell therapy closer to reality by providing translation-ready homogeneous cINs of the proper developmental stage for optimal grafting.

RESULTS

Optimization of Large-Scale Generation of MGE cIN Progenitors

In our previous study, we developed a protocol to generate homogeneous populations of cINs from hPSCs based on ventral specification of sphere or organoid culture.[18,26] For efficient use of hPSC-derived cINs, it is imperative to derive them in a scale large enough for industrial use in drug screening or cell therapy. Thus, we tested the effect of different methods of culture on the expansion and generation of MGE progenitors. The MGE progenitor cells were induced for three weeks according to our previous reports[14,18] with slight modifications (Figure S1A). After the establishment of sphere cultures under static conditions for a week, we tested three different culture conditions (static, shaker, and spinner) for 2 weeks. Spinner culture generated significantly greater increases in total cell numbers compared to static and shaker cultures (Figures 1A and 1B; Table S3). This is possibly due to more efficient air, nutrient, and waste exchange in the spinner system. Spinner culture also resulted in more homogeneous sphere sizes, without the random adhering of spheres that can cause spheres to become too big for efficient air, nutrient, and waste exchange (Figures 1A and 1B; Table S3). Next, we examined the phenotype of generated cells in each culture condition to rule out the possibility that spinner culture favors the induction or expansion of alternate phenotype cells with a faster growth rate than MGE progenitors. Despite massive expansion, cells grown in spinner culture also showed a homogeneous MGE progenitor phenotype shown by uniform NKX2.1 expression (Figures 1C and 1D). When further differentiated, cells from spinner culture generated homogeneous populations of cINs shown by uniform expression of SOX6, GAD1, and βIII-TUBULIN either as sphere cultures (Figures 1E and 1F) or after transferring to adherent cultures (Figure S1B). Some of the generated cINs expressed subtype-enriched markers such as MEF2C, SST, COUPTFII, and vasoactive intestinal polypeptide (VIP) (Figure S1C). There were very few other neural cells generated such as astrocytes ($GFAP^+$), oligodendrocytes ($OLIG2^+$), cholinergic neurons ($ChAT^+$), serotonergic neurons ($5HT^+$), dopaminergic neurons (TH^+), or glutamatergic neurons ($Glutamate^+$) (Figure S1C).

Long-Term Organoid Culture of cINs

Long-term culture of cINs was previously achieved by coculturing with the feeder cells such as astrocytes and glutamatergic neurons.[17,19,20,22] While feeder cells enable the long-term culture of generated human cINs, they may not be optimal for disease modeling or cell therapy. Thus, we tested whether we could maintain a homogeneous population of MGE cells as cIN spheres on a long-term basis without compromising the viability of the cINs. MGE spheres were maintained as spinner cultures for 6 weeks and then transferred to static culture to avoid shearing of organoids (Figure 2A). After 4 weeks

(n = 6–9 independent differentiations). (C and D) Spinner culture maintained the MGE progenitor phenotype. Cells were plated onto coverslips after 3 weeks' differentiation and analyzed for the MGE progenitor phenotype ($NKX2.1^+$) by immunocytochemistry (C) and cell counting (D). Scale bars, 50 μm. Data are presented as mean ± SEM (n = 3 independent differentiation). For the comparison of $NKX2.1^+$ cells, one-way ANOVA ($p = 0.171$) was performed. (E and F) MGE progenitors induced under different conditions generated cINs 6 weeks after differentiation, analyzed by immunocytochemistry (E) and cell counting (F). Scale bars, 50 μm. Data are presented as mean ± SEM (n = 3 independent differentiation). One-way ANOVA was performed for SOX6 ($p = 0.174$), GAD1 ($p = 0.708$), and βIII-TUBULIN expression ($p = 0.541$).

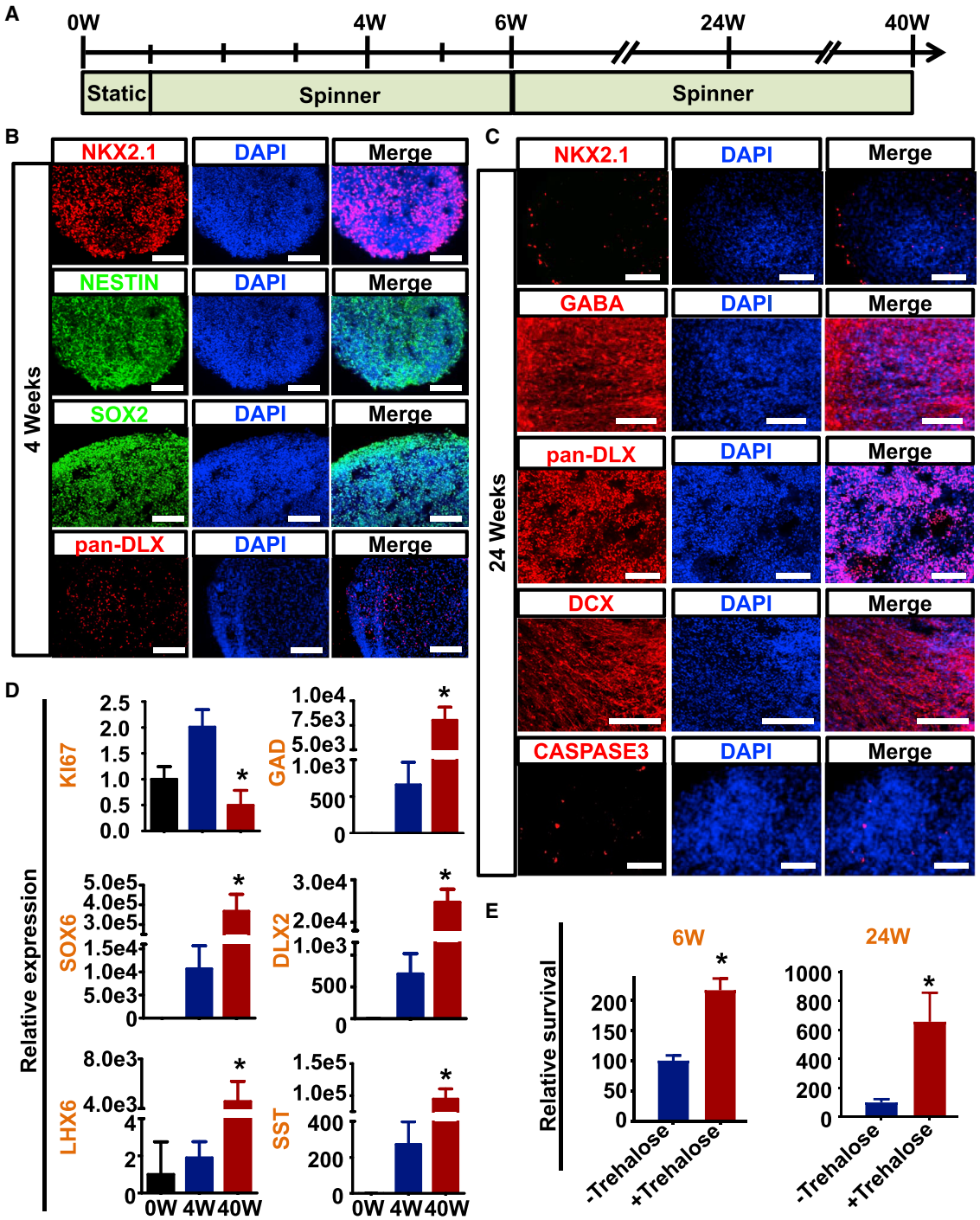

Figure 2. Long-Term Culture and Passaging of cIN Organoids

(A) Long-term culture scheme for the generation of cIN organoids. (B) Immunohistochemistry analysis of H9 cIN organoids after 4 weeks' differentiation for the MGE progenitor phenotype (NKX2.1, NESTIN, and SOX2) and cIN phenotype (pan-DLX). Scale bars, 100 μm. (C) Immunohistochemistry analysis of cIN organoids after 24 weeks' differentiation for the MGE progenitor marker (NKX2.1), cIN markers (GABA and pan-DLX), early postmitotic neuronal marker (DCX), and apoptosis marker (active CASPASE3). White scale bars, 100 μm. (D) Real-time PCR analysis of 4-week-old versus 40-week-old cIN organoids. Data are presented as mean ± SEM (n = 3 independent differentiation). For the comparison of gene expression, one-way ANOVA was performed for KI67 ($p = 0.027$), GAD1 ($p = 0.048$), SOX6 ($p = 0.003$), DLX2 ($p < 0.001$), LHX6 ($p = 0.022$), and SST ($p = 0.001$). The results of the Tukey post-hoc analysis are summarized in Table S4. (E) Trehalose efficiently increased the viability of the cINs during organoid passaging. Data are presented as mean ± SEM (n = 4 independent differentiation). Analysis was done using a two-tailed unpaired t test ($p = 0.006$ for 6 weeks and $p = 0.037$ for 24 weeks).

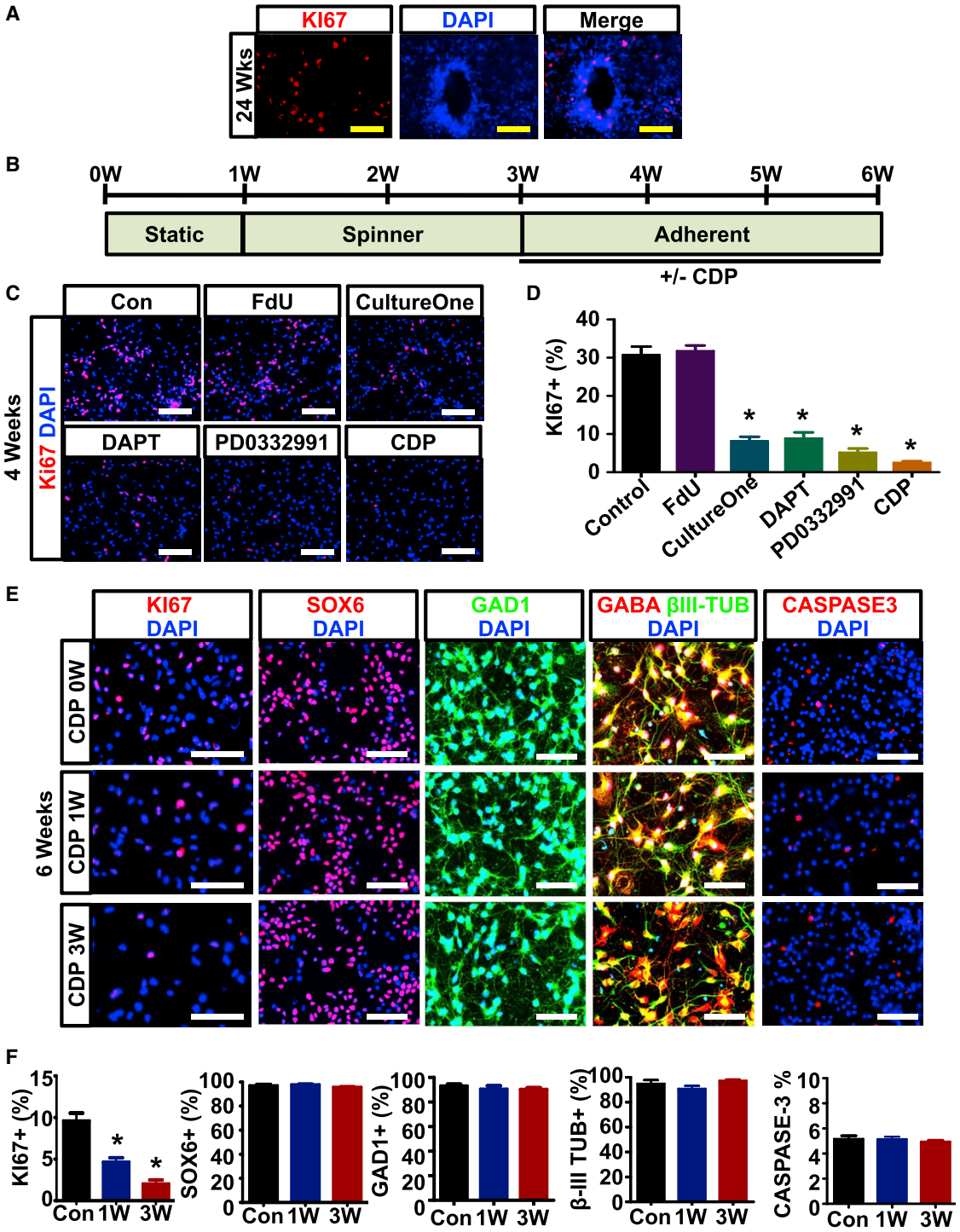

Figure 3. Combined Chemical Treatment Significantly Reduce Proliferating Progenitor Cells in cIN Culture

(A) Immunohistochemistry analysis of KI67^{+} proliferating progenitors in H9 cIN organoids 24 weeks after differentiation. Yellow scale bars, 50 μm. (B) Chemical treatment scheme for MGE progenitors. (C and D) Immunocytochemistry (C) and cell-counting analysis (D) of KI67^{+}-proliferating MGE progenitors after treatment with different chemicals for 1 week. Scale bars, 50 μm. For comparison of the proportion of proliferating cells, one-way ANOVA ($p < 0.001$) followed by Tukey post-hoc analysis was performed (Table S5). Data are presented as mean ± SEM (n = 4 independent differentiation). (E) Immunocytochemistry analysis of 6-week-old cINs treated with CDP for

(legend continued on next page)

of organoid culture, many cells expressed MGE progenitor markers, such as NKX2.1, NESTIN, and SOX2 (Figure 2B), whereas the proportion of pan-DLX$^+$ cells was relatively low. In MGE spheres after 24 weeks of culture, there were less NKX2.1$^+$ cells but more cells expressed the markers that are enriched in post-mitotic cINs such as GABA, pan-DLX, and DCX (Figure 2C). Spheres at 24 weeks of culture were still healthy without much sign of apoptosis (Figure 2C). We also quantitatively analyzed the changes in gene expression level as the cIN spheres matured by real-time PCR. Significant decreases in the expression of proliferating cell marker KI67 were observed as cIN spheres matured, whereas the expression of postmitotic cIN markers GAD, SOX6, DLX2, LHX6, and SST were significantly higher in 40-week-old cIN spheres compared to 4-week-old spheres (Figure 2D; Table S4).

One of the barriers of utilizing organoid culture for long-term maintenance of cINs is the difficulty of passaging older spheres or organoids, as they develop thick networks of neurites just as during normal brain development. Since it was reported that Trehalose could significantly improve cell viability after dissociation of neurons in mature mouse brains,[27] we tested the effect of Trehalose on the dissociation of tightly knit older spheres. Trehalose treatment during passaging significantly increased cell survival 6 weeks after differentiation. The increase in survival was much more pronounced in older spheres or organoids after 6 months' differentiation (Figure 2E). Optimized passaging of older spheres or organoids will enable the efficient utilization of cINs that are maintained long-term and feeder-free.

Combined Chemical Treatment Significantly Reduces Proliferating Progenitor Cells in cIN Culture

One thing we noticed in long-term organoid culture was the presence of proliferating cells (KI67$^+$) even 24 weeks after differentiation (Figure 3A). This population of lingering progenitors could generate grafts with uncontrolled growth when cells are used for cell therapy and could confound assays when postmitotic neurons are needed for disease modeling. Thus, we set out to optimize the culture to a more mature and postmitotic population, free of lingering proliferating progenitors. Thus, we treated 3-week-old MGE progenitors with various candidate chemicals or factors for a week and analyzed the proportion of proliferating cells (Figure 3B). The antimitotic drug fluorodeoxyuridine (FdU) did not influence the proportion of proliferating MGE progenitors, whereas neuronal culture supplement CultureOne, gamma secretase inhibitor N-[N-(3,5-difluorophenacetyl)-L-alanyl]-S-phenylglycine t-butyl ester (DAPT), or CDK4/6 inhibitor PD0332991 significantly reduced the proportion of proliferating progenitors. Furthermore, combined treatment of the three working chemicals (termed CDP) further decreased proliferating cells (Figures 3C and 3D; Table S5). As expected, the decrease in the proportion of proliferating cells was accompanied by a decrease in total cell number 1 week after CDP treatment (Figure S3). Extending CDP treatment to 3 weeks further reduced the proportion of proliferating progenitors compared to 1 week's treatment (Figures 3E and 3F; Table S6). The CDP treatment does not affect the phenotypes of treated cell populations (SOX6$^+$, GAD$^+$, and βIII-TUBULIN$^+$) or cell death even after 3 weeks' chemical treatment (Figures 3E and 3F).

Combined Chemical Treatment Facilitates the Synchronized Maturation of cIN Cultures

hPSC-derived cINs go through protracted maturation, recapitulating development *in vivo*.[18,19] Facilitating maturation to the proper stage will be important for efficient use of hPSC-derived cINs for disease modeling and cell therapy. To identify maturation parameters of cINs during development, we analyzed genes that are differentially expressed during their *in vivo* development, comparing cINs from E13.5 to adult brains.[28,29] One of the most striking changes during maturation of cINs in mouse brains was the significant upregulation of genes that regulated metabolism (Figures 4A and S4A). This developmental change makes sense, considering the high-energy demand of mature cINs. Thus, we analyzed metabolic maturation of cINs with or without CDP treatment using a seahorse analyzer (Figures 4B and S4B). CDP-treated cINs showed significant increase in oxidative phosphorylation, especially in basal respiration and ATP production (Figure 4C; Table S7).

During normal development of cINs, they migrate extensively from the MGE all the way to the dorsal telencephalon, where they make local synaptic connections and regulate local circuitry.[30] Thus, we tested whether CDP treatment can facilitate the transformation of MGE progenitors into actively migrating postmitotic cINs. Thus, we embedded 9-week-old cIN organoids in a Geltrex matrix with or without CDP treatment and analyzed their migratory properties 7 days after embedding (Figures 5A and 5B). There was a significant increase in migratory cINs by CDP treatment compared to untreated cells (Figures 5B and S5A).

As another criterion of maturation, we analyzed whether CDP treatment affects arborization of cINs. Three-week-old cINs were plated on coverslips and labeled only scarcely with a limiting titer of lentivirus that expresses GFP under the ubiquitin promoter (LV-Ubi-GFP). Arborization of CDP-treated or untreated cINs was analyzed after 3 weeks' CDP treatment (Figure 5A). There was a significant increase of arborization with CDP treatment (Figures 5C and S5B), shown by the increase in total neurite length and total branch numbers.

Next, we analyzed the electrophysiological maturation of cINs by whole-cell patch-clamp after 9 weeks' CDP treatment (Figure 5A).

0, 1, and 3 weeks. Scale bars, 50 μm. (F) Cell-counting analysis. One-way ANOVA ($p = 0.001$), followed by Tukey post-hoc analysis showed a significant decrease in KI67$^+$ cells after CDP treatment for 1 week ($p < 0.001$) and 3 weeks ($p < 0.001$) compared to the control group (Table S6). One-way ANOVA showed no significant difference among groups for SOX6$^+$ cells ($p = 0.985$), GAD1$^+$ cells ($p = 0.931$), βIII-TUBULIN$^+$ cells ($p = 0.896$), and active CASPASE3$^+$ cells ($p = 0.789$). Data are presented as mean ± SEM ($n = 5$ independent differentiation).

A

Term	Count	p-value	Benjamini
Metabolic pathways	182	4.0e-17	1.1e-14
Alzheimer's disease	36	4.2e-7	5.9e-5
Parkinson's disease	30	5.8e-6	5.4e-4
Oxidative phosphorylation	28	1.3e-5	8.8e-4
Arachidonic acid metabolism	21	1.9e-5	1.0e-3
Huntington's disease	34	4.0e-5	1.9e-3
Non-alcoholic fatty liver disease (NAFLD)	29	4.5e-5	1.8e-3
Steroid hormone biosynthesis	19	1.5e-4	5.3e-3

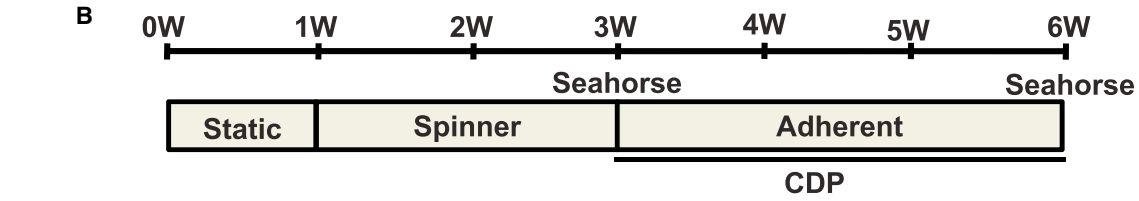

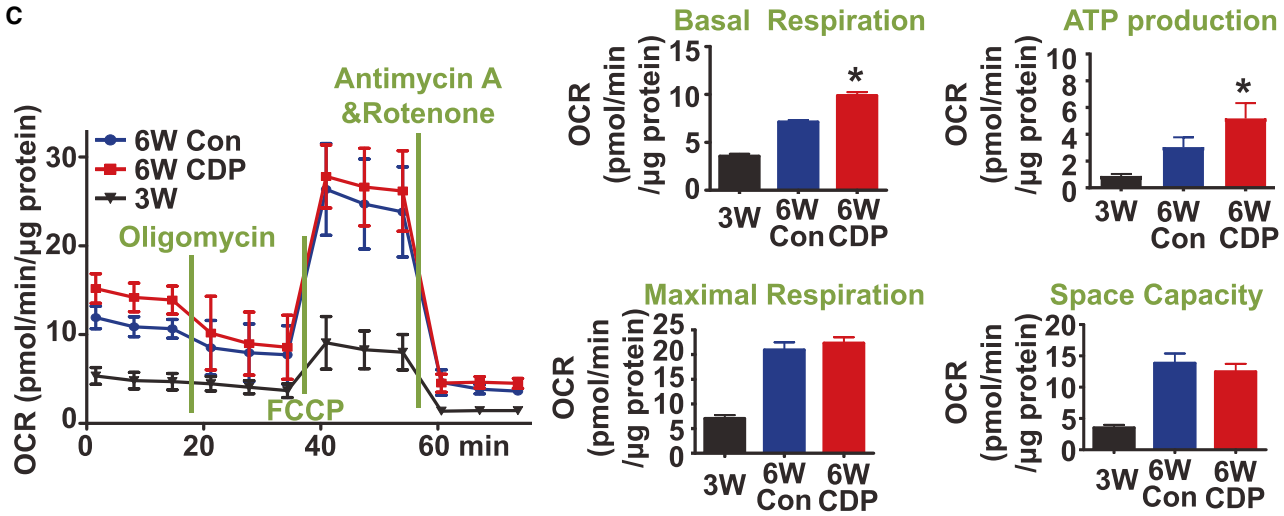

Figure 4. CDP Treatment Facilitates Metabolic Maturation of cINs

(A) DAVID analysis of genes with large differences in relative ranked expression between purified mouse cINs from E13.5 versus cINs from adult brain, showing significant changes in the metabolism pathway. (B) Analysis scheme for the metabolic maturation of cINs after CDP treatment. (C) CDP treatment significantly enhanced the metabolic maturation of H9 cINs. Data are presented as mean ± SEM (n = 10 wells) using paired one-way ANOVA. The Tukey post-hoc analysis was listed in Table S7.

CDP-treated cINs showed more mature membrane properties, including higher resting membrane potential (RMP), lower membrane resistance (Rm), and higher membrane capacitance (Cm). Of the cells recorded, a majority of cINs fired action potentials (APs), with an increased proportion of AP-firing neurons among those treated with CDP. CDP treatment also decreased AP threshold, but there was no significant difference in the parameters of AP firing, such as AP half width and afterhyperpolarization (AHP) (Figure S5C). We also analyzed 6-week-old cINs with 3 weeks' CDP treatment. The maturation of electrophysiological properties by CDP treatment was significant even at this time point (Figure S5D), with higher RMP, lower Rm, and higher Cm.

CDP-Treated cINs Generate Safe and Well-Integrating Grafts after Transplantation into Nod Scid Mouse Cortex

To further test the hypothesis that CDP-treated cINs will provide optimal populations for cell transplantation, we grafted 4-week-old cINs with or without a week of CDP treatment to Nod Scid mouse

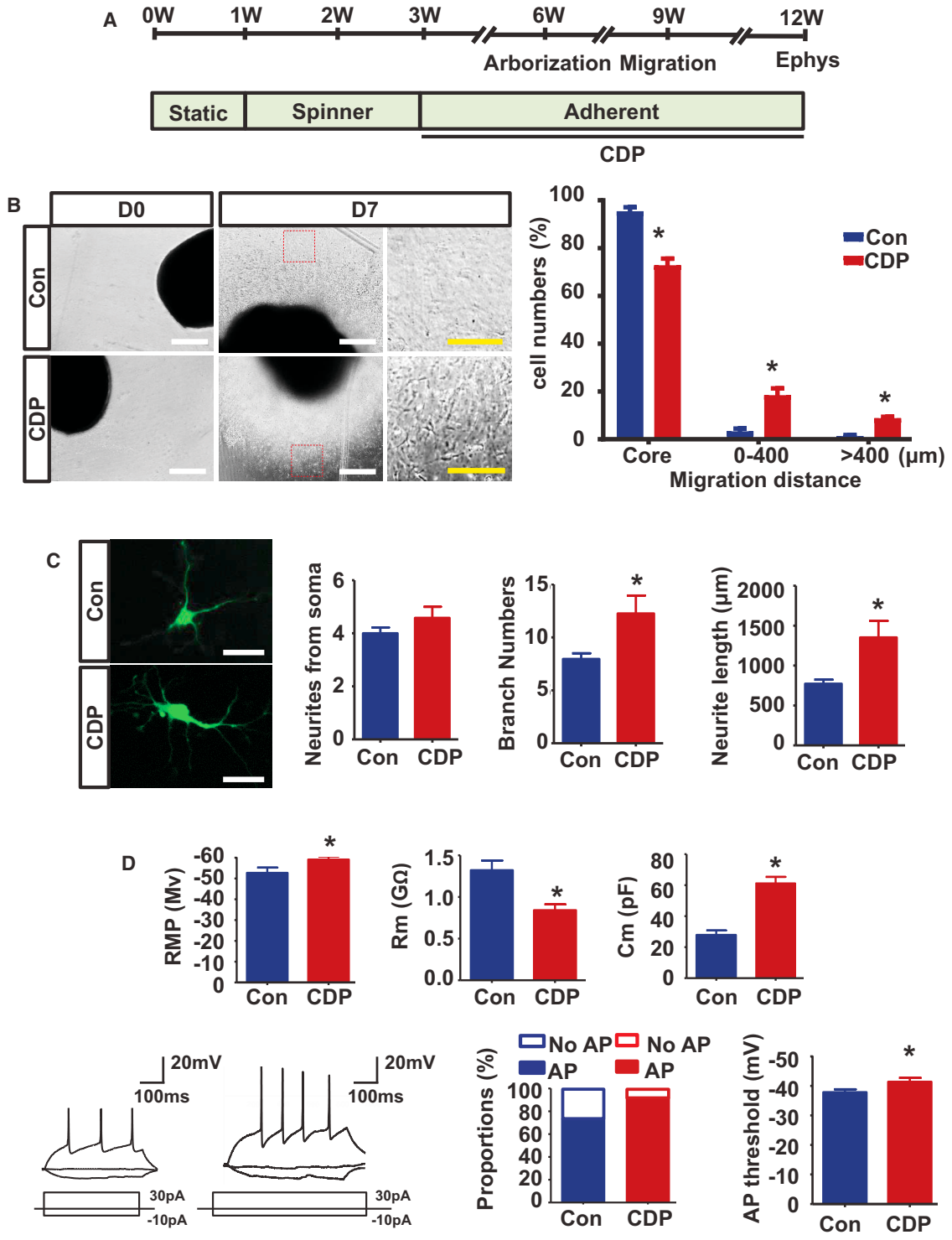

Figure 5. CDP Treatment Enhances Migratory, Morphological, and Electrophysical Maturation

(A) Analysis scheme for migration, arborization, and electrophysiology of cINs. (B) CDP treatment significantly increased the migration of generated iPSC cINs. cIN organoids were embedded in a Geltrex matrix at 9 weeks of differentiation with or without CDP treatment and analyzed for migration 7 days after embedding. White scale bars, 200 μm; yellow scale bars, 100 μm. Data are presented as mean ± SEM (n = 3 independent spheres). Analysis was done using a two-tailed unpaired t test ($p = 0.019$ for cells in the spheres, $p = 0.008$ for cells with migration distance of 0–400 μm, and $p = 0.001$ for cells with migration distance > 400 μm). (C) CDP treatment significantly enhanced

(legend continued on next page)

cortices and analyzed the grafts 1 month after transplantation (Figure 6A). Both untreated and CDP-treated cells generated grafts enriched with the MGE-derived cIN phenotype shown by ubiquitous expression of GABA and SOX6 (Figures 6B and 6C). Whereas there were still a number of KI67$^+$ proliferating cells in untreated grafts, such cells were rarely observed in CDP-treated cell grafts (Figures 6D and 6E). Consistent with having more proliferating cells in untreated cell grafts, the total graft cell numbers were significantly higher in untreated cell grafts compared to CDP-treated cell grafts (Figure 6E). This result gives confidence that CDP-treated cINs will generate safe grafts in the host brain without uncontrolled proliferation.

In addition, many more migrating cells were observed outside the graft core in CDP-treated cell grafts, whereas very few such cells were observed in untreated cell grafts at this time point (Figures 6D and 6F). Next, we tested the hypothesis that the CDP-treated cells, being more mature, would result in more efficient synapse formation of grafted cINs. Thus, we analyzed inhibitory synapse formation of grafted cINs by triple staining the grafted brains with antibodies against human-specific neural cell adhesion molecule (NCAM), inhibitory presynaptic marker vesicular GABA transporter (VGAT), and inhibitory postsynaptic marker Gephyrin. We then analyzed VGAT$^+$NCAM$^+$ puncta that were juxtaposed with Gephyrin$^+$ puncta using IMARIS software. There was a significant increase in inhibitory synapse formation among CDP-treated cINs in the host cortex compared to untreated cINs (Figures 6G and S6), suggesting CDP-treated cINs will provide cell populations for optimal integration into host circuitry.

Optimization of Cryopreservation of hPSC-Derived cINs

Considering the long-term culture required for cIN generation from hPSCs, the ability to freeze down and store intermediate progenies of differentiation will greatly enhance the efficiency of their utilization. It was reported that Trehalose could help pluripotent stem cells or other stem cells survive during cryopreservation.[27,31,32] Thus, we tested whether inclusion of Trehalose during cryopreservation of cINs can improve their viability (Figure 7A). Trehalose indeed significantly increased survival of cryopreserved cINs after freeze-thaw (Figure 7B) without affecting their phenotypes (Figures 7C and 7D). Under the optimized conditions, the majority of cINs maintained viability during cryopreservation under our optimized condition (65.27% ± 8.97% compared to the cINs passaged without cryopreservation). The phenotype of the cells was also well preserved during freeze-thaw cycles (Figures 7E and 7F).

DISCUSSION

Reliable and efficient generation of human cINs from hPSCs in large scale will be critical for further understanding interneuron-related brain disorders and the development of novel therapeutics. The fact that many therapeutics developed in animal models failed in human clinical trials[33,34] has raised the need to utilize real human tissues to develop novel therapeutics. In addition, large-scale reproducible generation of human cINs from hPSCs will be critical to the clinical realization of cell replacement therapy for interneuron-related disorders such as epilepsy, where novel therapeutics are desperately needed, especially for treatment-refractory patients. Previous studies provide a number of methods for generating cINs from hPSCs with varying efficiencies, some using genetic modification[20–22] and others by providing developmentally relevant signaling molecules.[6,17–19] However, large-scale generation of cINs that can support efficient drug screening and cell-transplantation therapy has not been reported so far. In this study, we have tested different methods of deriving MGE spheres and identified that spinner culture supports the generation of > 10-fold more MGE cells compared to the conventional static culture. The large increase was not due to overgrowth of irrelevant cell types, as we confirmed through immunocytochemical analysis, but more effective removal of cellular waste from the microenvironment surrounding spheres and efficient delivery of nutrients and oxygens by constant stirring. It was still surprising to observe a much greater generation of MGE cells compared to shaker culture, which is often used as an analogous method in many organoid cultures.[35–38] One thing we noticed was that using shaker culture, the spheres tended to adhere to each other and formed much larger clusters. This is likely due to centripetal force that tends to keep most of the spheres near the center of the flasks, whereas spheres from spinners form smaller and more homogeneous spheres, likely due to the shearing forces generated by the stirring motion. Thus, it is possible that the much larger size of shaker-based spheres prevented efficient circulation within spheres (removal of waste and delivery of nutrients and oxygen), whereas smaller and homogeneous spheres from spinners were more efficient.

To facilitate the maturation of MGE cells, we tested a series of agents that were implicated in cell cycle exit and maturation of neural cell types.[39–42] The antimitotic drug FdU was not effective in reducing immature proliferating cell numbers in MGE cell preparation. However, CultureOne supplement (Life Technologies), which is used to increase neuronal maturation, was effective in increasing the cell cycle exit of MGE cells. The gamma secretase inhibitor DAPT, which inhibits notch signaling and thus reduces neuronal progenitor proliferation[42–44] also worked well to control the cell cycle exit of MGE cells. The cyclin-dependent kinase 4/6 (CDK4/6) inhibitor PD0332991, which facilitates the cell cycle exit of proliferating neuronal progenitors[41] was also effective in regulating MGE cell cycle exit. A combination of the last three chemicals was more effective in inducing the synchronous maturation of MGE cells than any single

arborization of H9 cINs. Number of neurites from soma ($p = 0.180$), branch numbers ($p = 0.001$), and neurite lengths ($p = 0.005$) were analyzed by two-tailed unpaired t test. Data are presented as mean ± SEM (n = 12 neurons). (D) CDP treatment significantly enhanced the electrophysiological maturation of cINs after 9 weeks' CDP treatment. Data are presented as mean ± SEM (n = 24 control neurons and n = 28 CDP-treated neurons). Analysis was done using a two-tailed unpaired t test for resting membrane potential (RMP; $p = 0.041$), membrane resistance (Rm; $p = 0.001$) and membrane capacitance (Cm; $p < 0.001$). CDP treatment generated a higher proportion of neurons with action potential firing (Chi-square test; $p = 0.001$) with significant increase of AP threshold ($p = 0.046$).

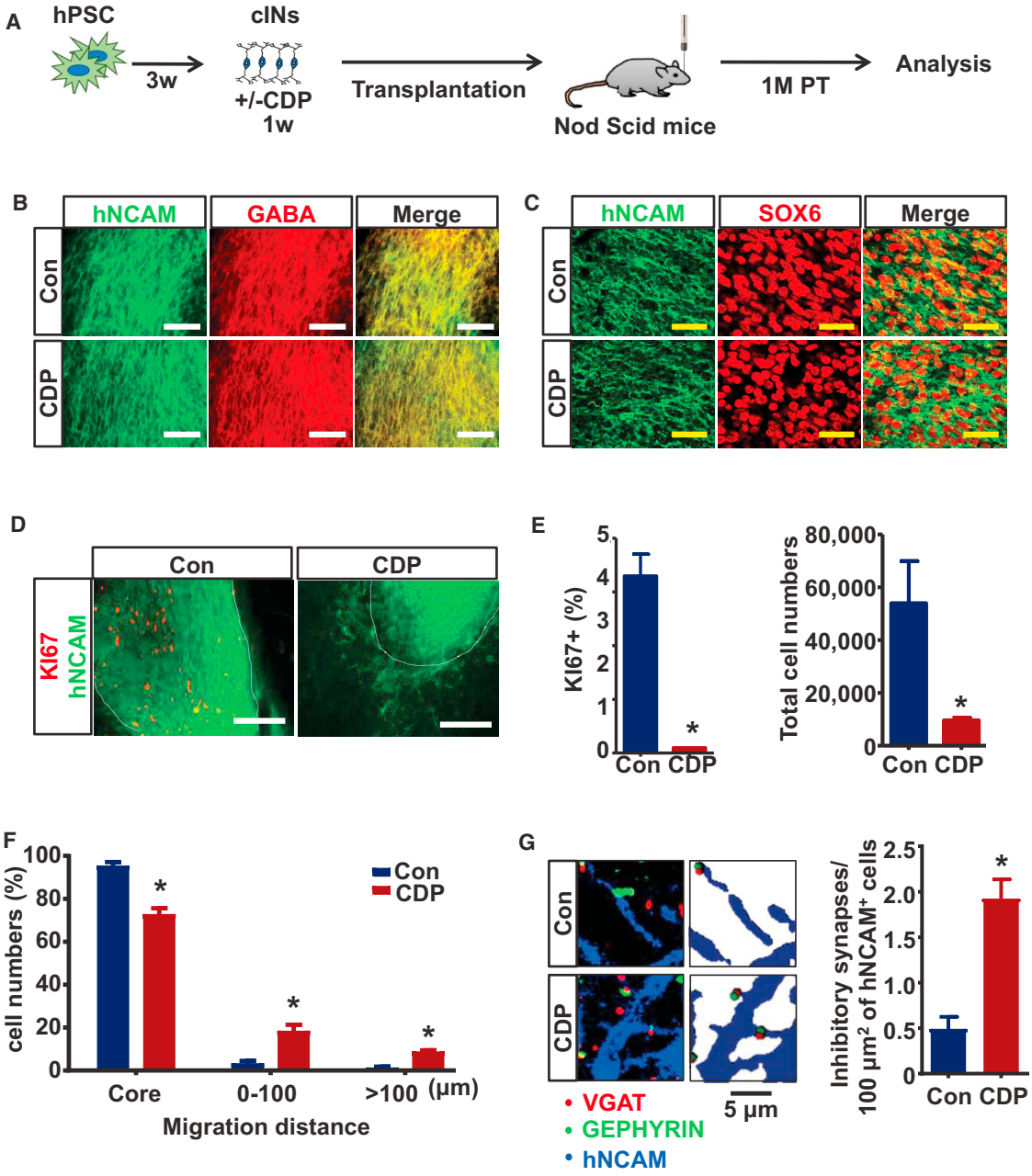

Figure 6. Transplantation Analysis of CDP-Treated cINs after Transplantation into Nod Scid Mouse Cortex

(A) Scheme of transplantation analysis. cINs with or without 1 week's CDP treatment were transplanted into the cortex of Nod Scid mice, and grafts were analyzed 1 month after transplantation. (B and C) Untreated or CDP-treated H9 cells generate grafts enriched with MGE-type cINs, as shown by immunohistochemistry analysis using anti-GABA antibody (B) and anti-Sox6 antibody (C). White scale bars, 50 μm, and yellow scale bars, 25 μm. (D) CDP-treated cINs generated grafts with a lower proportion of proliferating cells, as analyzed by immunohistochemistry using antibodies against human-specific NCAM and KI67. The white dotted lines mark the graft borders. Scale bars, 100 μm. (E) CDP treatment significantly decreased the proportion of proliferating cells in the graft 1 month after transplantation ($p < 0.001$) and the total graft cell numbers ($p = 0.049$). Data are presented as mean ± SEM ($n = 4$). Analysis was done using a two-tailed unpaired t test. (F) Migration analysis of grafted cINs. Data are presented as mean ± SEM ($n = 3$). Analysis was done using a two-tailed unpaired t test ($p = 0.002$ for cells in graft core, $p = 0.008$ for cells with migration distance 0–100 μm, and $p = 0.001$ for cells with migration distance > 100 μm). (G) Analysis of inhibitory GABAergic synapses in grafted cINs 1 month after transplantation. Scale bar, 5 μm. Data are presented as mean ± SEM ($n = 5$). Analysis was done using a two-tailed unpaired t test ($p < 0.001$).

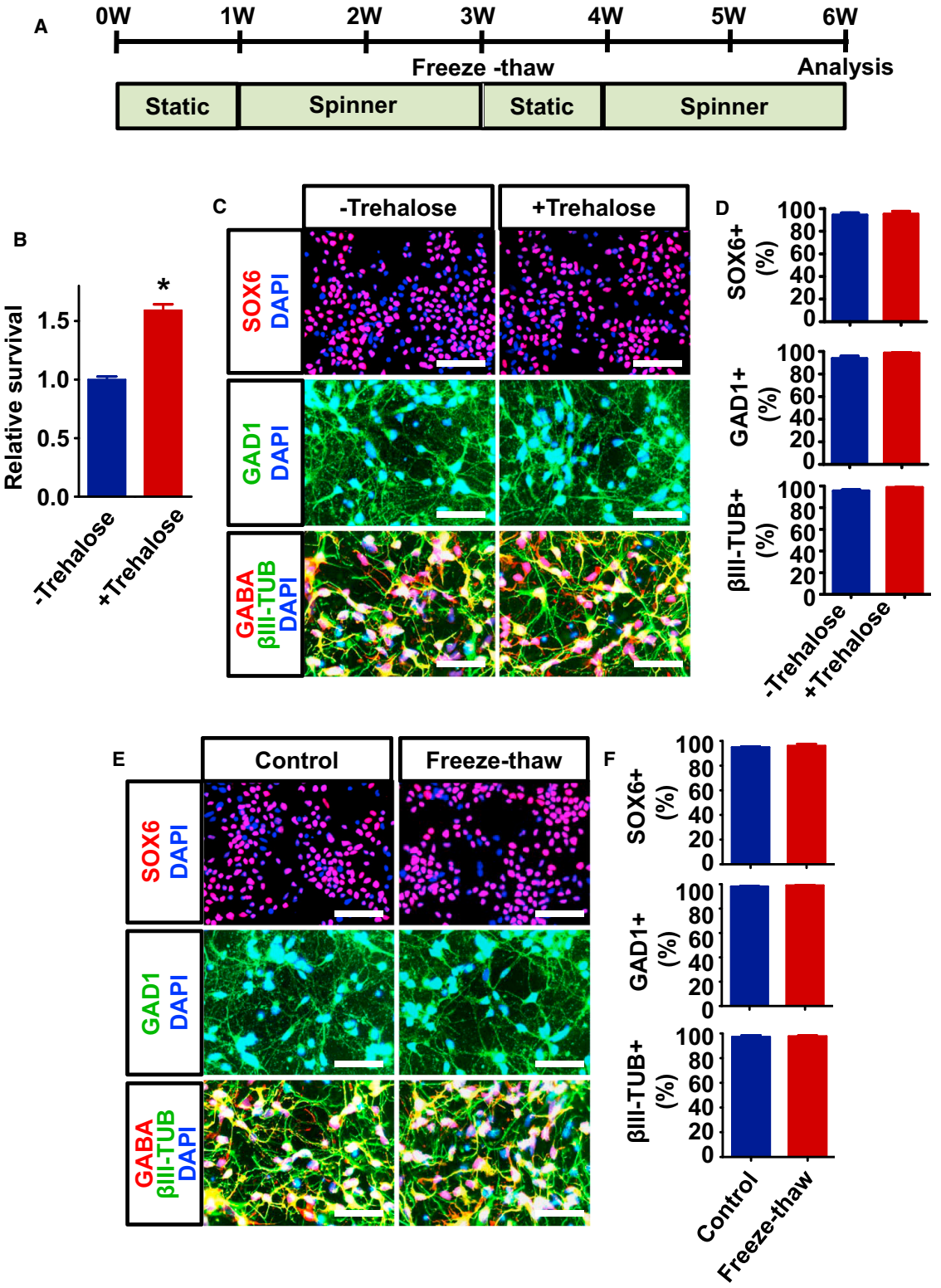

Figure 7. Cryopreservation of MGE Progenitors

(A) Analysis scheme of MGE progenitor cryopreservation. (B) Trehalose in freezing media increased the H9 cIN survival during cryopreservation. cIN progenitors were trypsinized after 3 weeks' differentiation, and the same number of cells were frozen with or without Trehalose in freezing media. Total cell numbers were counted after

(legend continued on next page)

treatment with each chemical alone. Previously, genetic modification has been used to facilitate MGE phenotype induction or faster maturation.[20–22] However, genetic modification methods need to be used with caution for studying diseases with complex genetics such as schizophrenia, where hundreds of common variants (single nucleotide polymorphisms [SNPs]) work together to cause the phenotype.[45] Thus, a method that could change the SNP landscape would not be desirable. Furthermore, more caution will be needed to generate clinical-grade cell populations for the purpose of cell therapy to avoid potential insertional mutations in the grafted cells. Other studies employed feeder coculture such as astrocytes or glutamatergic neurons for better maturation and maintenance.[17,19,20,22] Feeder-based cultures also could hinder analysis where a pure population is more desirable (such as transcriptome analysis applications) and may not be optimal, especially for clinical applications that require xeno-free preparation of cells. Thus, in this study, we used a chemical combination without the use of genetic modification or feeder coculture to facilitate the functional maturation of cINs (metabolism, migration, arborization, and electrophysiology). Such enhanced maturity will be important for both drug-screening purposes and to reduce the time, cost, and effort necessary to generate cell populations sufficiently mature for assays. In addition, as shown in this study, this enhanced maturation will also be critical to avoid uncontrolled growth of proliferating cells in grafts and better integration of grafted cells into the host brain with superior migration, arborization, and synaptic connection. One caveat is that although we observed en masse "maturation" of cINs in diverse physiological aspects, we cannot distinguish whether we promote maturation from "proliferating MGE progenitors" to "postmitotic" cINs only or also maturation from "immature cINs" to "more mature cINs." This could be addressed by employing single-cell RNA-seq in the future.

It is well-known that human cINs derived from hPSCs are undergoing protracted maturation comparable to their *in vivo* developmental timeline. Continued maturation has been observed during the culture of hPSC-derived cINs just as during normal development,[18,19] and our protocol with chemical treatment significantly facilitates this process. Some applications of hPSC-derived cINs, such as modeling the disease phenotype in adult brains, will require the attainment of a fully mature phenotype. However, for the purpose of cell therapy, this type of developing migratory cIN ($SOX6^+$ $KI67^-$) will be more beneficial than completely mature neurons in that (1) completely mature neurons with elaborate neurites will be more vulnerable to the passaging and transplantation procedure than developing cINs and (2) completely mature neurons lack the migratory properties necessary for optimal integration into host circuitry, unlike these developing early postmitotic cINs. They will also be better suited for cell therapy compared to more immature progenitors in that (1) they contain all the machinery to readily integrate into and regulate host circuitry and (2) they are postmitotic without any more proliferating cells that would increase the chance of uncontrolled growth of grafted cells. Overall, in this study, we have shown efficient large-scale generation of hPSC-derived human cINs with the proper developmental stage optimal for cell transplantation, and this work will provide critical tools for efficient use of hPSC-derived cINs for cell therapy.

MATERIALS AND METHODS

Culture of hPSC and Differentiation into cINs

These study protocols were approved by the New York Medical College Institutional Review Board. All procedures were performed in accordance with the institutional review board's guidelines.

Human embryonic stem cell (hESC) line H9 (WiCell, Madison, WI, USA, passage 30–50) or iPSC lines 272, 190, and 483[46] was maintained on Geltrex (Thermo Fisher, Waltham, MA, USA)-coated plates in Essential 8 medium (Thermo Fisher, Waltham, MA, USA). ROCK inhibitor (Y27632, 10 μM, ApexBio, Boston, MA, USA) was added to the culture for 24 h after passaging to prevent single-cell-induced cell death of hPSCs. All the chemicals used in this study were listed in Table S1.

MGE differentiation was initiated by passaging H9 cells as spheres in low adherent flasks with SRM media (DMEM with 15% knockout serum replacement [KSR], 2 mM L-glutamine and 10 μM β-mercaptoethanol [all from Thermo Fisher, Waltham, MA, USA]). ROCK inhibitor was also included on the day of differentiation. For the first week, cells were differentiated in SRM LSsgW media (the SRM media supplemented with 0.1 μM LDN193189 [Selleck Chem, Houston, MA, USA], 10 μM SB431452 [Tocris Bioscience, Minneapolis, MN, USA], 0.1 μM SAG [Selleck Chem, Houston, MA, USA], and 5 μM IWP2 [Selleck Chem, Houston, MA, USA]). For the second week, SRM Lsg media (the SRM media was supplemented with 0.1 μM LDN193189 and 0.1 μM SAG) was used. In the third and fourth weeks, the media was changed to N2AA media (DMEM/F12 media with 0.5% N2 supplement [Life Technologies, Woburn, MA, USA], and 200 μM AA-ascorbic acid [Sigma-Aldrich, Natick, MA, USA]). For the third week, the N2AA media was supplemented with 0.1 μM SAG and 50 ng/mL FGF8 (ProSpect, Rocky Hill, CT, USA). At the beginning of the fourth week, the N2AA media was

3 weeks' recovery from cryopreservation as a sphere culture. Data are presented as mean ± SEM (n = 4 independent differentiation). Analysis was done using a two-tailed unpaired t test ($p < 0.001$). (C and D) Trehalose treatment during the freeze-thaw cycle did not alter the cIN phenotype, analyzed by immunocytochemistry (C) and cell counting (D). The cINs were analyzed 3 weeks after thawing by immunocytochemistry for cIN marker expression (SOX6, GAD, and βIII-TUBULIN). Scale bars, 50 μm. Data are presented as mean ± SEM (n = 4 independent differentiation). Analysis was done using a two-tailed unpaired t test (SOX6, $p = 0.797$; GAD, $p = 0.128$; βIII-TUBULIN, $p = 0.063$). (E and F) The optimized cryopreservation protocol maintained cIN phenotype well comparable to the cells without cryopreservation, analyzed by immunocytochemistry (E) and cell counting (F). The cINs, 3 weeks after thawing, were analyzed for the cIN phenotypes (SOX6, GAD, and βIII-TUBULIN) by immunocytochemistry. Scale bars, 50 μm. Data are presented as mean ± SEM (n = 4 independent differentiation). Analysis was done using a two-tailed unpaired t test (SOX6, $p = 0.743$; GAD, $p = 0.765$; βIII-TUBULIN, $p = 0.391$).

supplemented with 5 ng/mL glial cell line-derived neurotrophic factor (GDNF) (ProSpect, Rocky Hill, CT, USA), and 5 ng/mL brain-derived neurotrophic factor (BDNF; ProSpect, Rocky Hill, CT, USA) (N2AAGB media). From the fifth week, the cells were maintained in the B27GB media (DMEM/F12 media with 1% B27 supplement [Thermo Fisher, Waltham, MA, USA], 5 ng/mL GDNF, and 5 ng/mL BDNF). For comparison of different culture conditions, cells were cultured in the flask as a static culture or shaking on orbital shaker at 80 rpm (SK-O180-E analog orbital shaker, Scilogex, Rocky Hill, CT, USA) or using stirrer culture system at 80 rpm (Celstir spinner flask [Wheaton, Millville, NJ, USA] and Multistirrer Digital Series Magnetic Stirrers (VELP Scientifica Srl, MB Italy). All cell lines were routinely tested for mycoplasma once a week using a mycoplasma detection kit (InvivoGen, San Diego, CA, USA).

For passaging cINs, cells were trypsinized by 0.05% trypsin (Thermo Fisher, Waltham, MA, USA) supplemented with or without 100 mM Trehalose (Sigma-Aldrich, Natick, MA, USA). After 5 min incubation at 37°C, the spheres were triturated to dissociate the spheres. An equal volume of DMEM media with 10% FBS (Hyclone, Marlborough, MA, USA) was added to neutralize Trypsin. In addition, Turbo DNase (2 U/mL, Thermo Fisher, Waltham, MA, USA) was added to help clear released DNAs from culture. The cells were then kept in the incubator for additional 15 min to remove any sticky DNA mass released during trituration. After incubation, the cells were centrifuged and resuspended by B27GB media with ROCK inhibitor. To exclude the dead cell cluster, the resuspended cells were filtered through a cell strainer cap (35-μm nylon mesh, Corning, NY, USA) and plated onto a PLO/FN-coated surface (poly-L-ornithine, 15 μg/mL, Sigma-Aldrich, Natick; fibronectin, 10 μg/mL, Thermo Fisher, Waltham, MA, USA) for the subsequent experiments.

For chemical treatment of cINs, the differentiated progenitors were seeded on PLO/FN-coated surface at 3 weeks after differentiation, and cultured in B27GB media without or with each chemical, 20 μM FdU (Sigma-Aldrich, Natick, MA, USA), 1% CultureOne (C, Thermo Fisher, Waltham, MA, USA), 10 μM DAPT (D, Sigma-Aldrich, Natick, MA, USA), and 2 μM PD0332991 (P, Sigma-Aldrich, Natick, MA, US), or with combination of CultureOne, DAPT, and PD0332991 (CDP) for the time period designated in each figure.

For cryopreservation, the trypsinized cells were resuspended in freezing media (fetal bovine serum [FBS] with 10% DMSO) with or without 100 mM Trehalose and were frozen slowly overnight in an insulated container at −80°C deep freezer. After 24 h, the stocks were moved to liquid nitrogen storage until further experiments. Frozen stocks were thawed quickly in a 37°C water bath, transferred to 15 mL conical tubes with 5 mL media, centrifuged, and resuspended in B27GB media with ROCK inhibitor for plating and further experiments.

Immunocytochemistry and Cell Counting

cINs on coverslips were fixed using 4% paraformaldehyde (PFA; Electron Microscopy Sciences, Hatfield, PA) for 10 min, washed with PBS, and used for staining. The spheres at different differentiation stages were fixed by 4% PFA for 15 min, rinsed with PBS, cryo-protected in the 30% sucrose (Thermo Fisher, Waltham, MA, USA) overnight at 4°C, mounted on the chuck using the optimum cutting temperature (OCT) compound (Thermo Fisher, Waltham, MA, USA) and cryosectioned at 40 μm using a Leica CM1850 cryostat (Leica Biosystem, Buffalo Grove, IL, USA). Fixed cells or sphere sections were incubated with blocking and permeablization buffer (PBS with 10% normal serum and 0.1% Triton X-100) for 10 min. The samples were then incubated in primary antibodies in antibody dilution buffer (PBS containing 2% normal serum) overnight at 4°C. The detailed information of the antibodies used were listed in Table S2. After washing with PBS, cells were incubated with fluorescently labeled secondary antibodies and DAPI (Invitrogen, Waltham, MA, USA) in antibody dilution buffer for 1 h at room temperature. Following the PBS wash, the samples were mounted with fluoromount-G (SouthernBiotech, Birmingham, AL, USA).

Fluorescent images were taken by the EVOS FL auto microscope (Life Technologies, Carlsbad, CA), Olympus DSU Spinning Disc Confocal on an IX81 inverted microscope (Olympus, Center Valley, PA, USA), and Zeiss LSM710 confocal laser-scanning microscopes (Zeiss, Oberkochen, Gremany).

For cell counting, multi-point function in ImageJ software (Version 1.51p, NIH, Bethesda, MD, USA) was used. Percentage of positive cells for each marker was calculated by dividing by DAPI-stained total nuclei number from at least three separate biological replicates. For each staining, a total of at least 500 cells were counted for each group.

RNA Preparation, Reverse Transcription, and Real-Time PCR Analysis

Cells were harvested using TRIzol (Thermo Fisher, Waltham, MA, USA), and total RNAs were prepared according to the manufacturer's protocol. For the reverse transcription, 500 ng total RNA was first reversely transcribed to cDNA using RevertAid H Minus Reverse Transcriptase (Thermo Fisher, Waltham, MA, USA). The real-time PCR reaction was carried out in a 96-well format with SsoAdvanced Universal SYBR Green Supermix (Bio-Rad, Hercules, CA, USA). The primer information is as follows: KI67 (F 5′-TCCTTTGGTGGGCACCTAAGACCTG-3′, R 5′-TGATGGTTGAGGTCGTTCCTTGATG-3′), GAD (F 5′-CTGCTCTTCTCTTACGCTCTCTGTC-3′, R 5′-TCTTCGGAAATGTTGCCTTAGG-3′), SOX6 (F 5′-ATCTCTCATCCCGACCCAAGAC-3′, R 5′-TTCCCAGGCTTCCTCCAATG-3′), DLX2 (F 5′-GCCTCAACAACGTCCCTTACT-3′, R 5′- GGGAGCGTAGGAGGTGTAGG-3′), LHX6 (F 5′-ATTCCTTGCGTGGATTATGTGG-3′, R 5′-TCCGTGTGTGTGTTTTCCCC-3′), SST (F 5′-CAGGATGAAATGAGGCTTGAGC-3′, R 5′-TTAGGGAAGAGAGATGGGGTGTGG-3′), and GAPDH (F 5′-GCTCAGACACCATGGGGAAGGT-3′, R 5′-GTGGTGCAGGAGGCATTGCTGA-3′). All reactions were carried out and analyzed using the CFX96 real-time PCR system (Bio-Rad, Hercules, CA, USA). The expression of GAPDH mRNA in each sample was used

to normalize the data. Relative gene expression was analyzed by $2^{-\Delta\Delta Ct}$ method.

Identification of cIN Maturation-Specific Rank-Based Differences in Gene Expression

To identify transcriptome changes during cIN maturation, we compared the transcriptome of purified cINs in the E13 mice cortex[28] versus purified cINs in the P40 mice cortex.[29] All MoGene 1.0 ST arrays[28] were processed using the "oligo" BioConductor package[47] and all mouse 430A2 arrays[29] with the "affy" Bioconductor package.[48] Both the E13 cortex and P40 interneurons' array data were quality controlled with array Quality Metrics,[49] normalized with multi-array average (RMA),[50] filtered, subset to one probe per gene (using the probeset for each gene with the maximum mean value for all samples) and further subset to common genes between two datasets using the insilicodb Bioconductor package.[51] Due to difference in the probe intensity distributions of the two arrays in the studies, we compared gene expression via a rank-based method. In brief, rank-based analysis was performed as follows: expression intensities for each gene were ranked within each sample and squared. The mean squared ranks for a study were then compared to find genes with the high expression in adults and low expression in embryonic samples. Pathways enriched after cIN maturation (rank difference > 3,000) were identified using DAVID (https://david.ncifcrf.gov/).

Oxidative Phosphorylation Analysis Using Seahorse Analyzer

Mitochondrial activity of cINs was measured using the seahorse XFp8 analyzer (Agilent Technologies, Santa Clara, CA, USA) according to the manufacturer's instructions. In brief, cells were plated in the XF cell culture miniplate and incubated at 37°C with 5% CO_2. One day before the test, the cartridge with XF calibrant was incubated in a non-CO_2 incubator overnight to equilibrate. Before the assay, the media was changed to XF assay medium supplemented with 5 mM sodium pyruvate (Thermo Fisher, Waltham, MA, USA), 10 mM glucose (Thermo Fisher, Waltham, MA, USA), and 2 mM glutamine and equilibrated in a non-CO_2 incubator for 1 h. Oxygen consumption rates (OCRs) were monitored through sequential injections of 1 μM oligomycin, 0.3 μM carbonyl cyanide 4-(trifluoromethoxy) phenylhydrazone (FCCP), and 1 μM rotenone/antimycin A (seahorse XF cell mito stress test kit, Agilent, Santa Clara, CA, USA). Raw data were used to calculate the various parameters of the mitochondrial activity: basal respiration = baseline OCR-rotenone/antimycin A OCR; ATP production = baseline OCR-oligomycin OCR; maximum respiration = FCCP OCR-rotenone/antimycin A OCR; and spare capacity = maximum respiration-basal respiration. The result was normalized to total protein levels quantified using a bicinchoninic acid (BCA) protein assay (Thermo Fisher, Cambridge, MA, USA).

cINs Migration and Arborization Analysis *In Vitro*

For *in vitro* migration analysis, 9-week-old cIN spheres were embedded in Geltrex matrix and treated with or without CDP for 7 days. Phase pictures were taken on day 0 and day 7 after embedding to follow migration of cINs. For quantification of migrated cells, the embedded spheres were incubated with Hoechst (Sigma-Aldrich, Natick, MA, USA) overnight on day 7, and the entire embedding was imaged and tiled for Hoechst signal and used for cell counting using the multi-point function in ImageJ software. Cell numbers within sphere core, in migration distance 0–400 μm, and in distance longer than 400 μm were counted separately for each sphere.

For arborization analysis, the MGE progenitors were plated onto the PLO/FN-coated coverslips after 3 weeks' differentiation with or without CDP. Two weeks later, the MGE cells were infected with limiting titer (MOI, 0.001) of LV-UbiC-GFP virus[52] to label cells only scarcely. One week after infection, the images of GFP^+ cells were collected by the EVOS microscope. The arborization of each GFP^+ cell was analyzed using ImageJ software with the Neuron J plugin to get parameters of total neurite length, total branch number, and neurite number from soma.

Electrophysiological Analysis *In Vitro*

Three-week-old MGE progenitor cells were cocultured on PF-coated coverslips with rat cortical astroglial cells (PC36108, Neuromics, Edina, MN, USA) at a ratio of 5:1 and in B27GB media supplemented with 1.8 mM $CaCl_2$. cINs were then infected with a LV-Syn-Chr2-YFP virus (plasmid #20945, Addgene, Cambridge, MA, USA) and maintained with or without CDP treatment for 9 weeks. At 12 weeks, cINs were transferred into a recording submersion chamber, which was continuously perfused at room temperature (21°C –23°C) at a flow rate of 1.5–2 mL/min with artificial cerebrospinal fluid (130 mM NaCl, 2.5 mM KCl, 2.5 mM $CaCl_2$, 1 mM $MgSO_4$, 1.25 mM NaH_2PO_4, 26 mM $NaHCO_3$, and 10 mM glucose) with an osmolarity of 295–305 mM, gassed continuously with 5% CO_2/95% O_2. Whole-cell patch-clamp recordings were acquired with a Multiclamp 700B (Axon Instruments, Molecular Devices, San Jose, CA, USA), Digidata 1550 (Axon Instruments, Molecular Devices, San Jose, CA, USA), and Clampex 10 software (Molecular Devices, San Jose, CA, USA). Whole-cell patch-clamp electrodes (3–5 mΩ resistance) were filled with an intracellular solution containing in mM: 120 K-gluconate, 9 KCl, 10 KOH, 8 NaCl, 10 HEPES, 3.48 MgATP, 0.4 Na_3GTP, 17.5 sucrose, 0.5 EGTA, with an osmolarity of ~290 and pH 7.3. Sampling was done at 5 kHz unless specified otherwise. Liquid junction potential of 9.7 mV was corrected for the internal pipette solution used. RMP was recorded at I = 0. To compare membrane excitability, membrane potential was held at −70mV and square pulses of depolarizing current steps were applied in current clamp mode (−10 to −80 pA in increments of 10 pA, 0.8 s duration). The first AP induced by depolarizing current was used to analyze AP threshold, AHP amplitude, and AP half-width, using Clampfit software (Molecular Devices, San Jose, CA, USA). Cm was calculated with the membrane test function on Clampex 10, using a 5 mV voltage pulse from the holding voltage of −70 mV and recorded currents in voltage-clamp mode with a sampling rate of 100 kHz. Rm was calculated in current clamp mode by applying a −10 pA current step and using the steady-state voltage deflection to calculate Rm as (steady-state voltage deflection/−10 pA). Averages ± SEM are represented in Figures 5 and S5B.

cINs were also split after 3 weeks' differentiation without feeder cells. After treated with or without CDP for 3 weeks, the electrophysiology analysis was performed as described above. Averages ± SEM of these cells are represented in Figure S5C.

Transplantation and Immunohistochemistry Analysis

All animal procedures were carried out in accordance with the approved guidelines and all animal protocols were approved by the Institutional Animal Care and Use Committee at New York Medical College. The cINs were trypsinized and plated on a PLO/FN plate at the density of $10^5/cm^2$ at the end of 3 weeks' differentiation. After 1 week's CDP treatment, the cINs were trypsinized and resuspended in transplantation media (Hank's balanced salt solution [HBSS] with 4.5 mg/mL sucrose, 10 ng/μL GDNF, 10 ng/μL BDNF, 20 nM Boc-Asp(OMe) fluoromethyl ketone [BAF; Sigma-Aldrich, Natick, MA, USA], and 10 μM rock inhibitor at a density of $1 \times 10^5/\mu L$). A 1-μL volume of cINs were injected into the cortices of Nod Scid mice (Charles River Laboratory, Kingston, NY, USA) using a Kopf stereotaxic instrument (Kopf, Tujunga, CA, USA) with a mouse adaptor (Stoelting, Wood Dale, IL, USA) under isoflurane anesthesia (3% induction, followed by 1% maintenance). The cells were injected at each of the following coordinates: AP 0.00 mm, L ± 3.28 mm, V −1.80 mm; AP −2.12 mm, L ± 4.20 mm, V −2.00 mm. One month after transplantation, the mice were perfused with 0.1 M PBS followed by 4% PFA. The brains were removed and postfixed in 4% PFA solutions overnight and then placed in 30% sucrose solutions for 1 day. Forty-micrometer-thick coronal sections were cut on a Leica CM1850 cryostat (Leica Biosystem, Buffalo Grove, IL, USA). The immunohistochemistry process followed the same procedure as immunocytochemistry as described above. The antibodies used are summarized in Table S2. Images were captured and analyzed by EVOS FL auto microscope (Life Technologies, Carlsbad, CA, USA) and Zeiss LSM710 confocal laser scanning microscopes (Zeiss, Oberkochen, Gremany).

For *in vivo* migration analysis, human-specific NCAM/DAPI images of areas including more than 500 μm around the graft were captured and tiled using Zeiss LSM710 confocal laser scanning microscopes with 10× objective, and grafted cell numbers were counted using the multi-point function in ImageJ software. Grafted cells in the graft cores, in migration distance of 0–100 μm and in migration distance longer than 100 μm were counted separately for each graft.

For synapse analysis, images were captured using Zeiss LSM710 confocal laser scanning microscopes (Zeiss, Oberkochen, Gremany) with 100× objective and processed using IMARIS software (Bitplane, Switzerland), which allows objective counting of synaptic puncta based upon absolute fluorescent intensity. Synaptic puncta positive for VGAT (inhibitory presynaptic) and Gephyrin (inhibitory postsynaptic) were identified with spot diameters of 0.6 μm. For synapses, a juxtaposition of $hNCAM^+VGAT^+$ puncta and $Vglut1^+$ puncta was determined as inhibitory synapses. The result was expressed as synapse numbers per human $NCAM^+$ neuronal surface area (μm^2). We analyzed a total of 795 neurite segments with a total area of 7,442 μm^2 for control cINs and a total of 977 neurite segments with a total area of 7,442 μm^2 for CDP-treated cINs. Total counted colocalized puncta numbers are 37 for control cINs and 161 for CDP-treated cINs.

Statistics

The statistical analysis was performed using GraphPad Prism7 (GraphPad Software, La Jolla, CA, USA). A two-tailed, unpaired t test was used to compare the difference between two groups. One-way ANOVA was used to compare the difference among multiple groups, and once a significant difference was observed, Tukey post-hoc test was performed to compare the difference between any two groups. When $p < 0.05$, the difference was considered as statistically significant.

SUPPLEMENTAL INFORMATION

Supplemental Information can be found online at https://doi.org/10.1016/j.omtm.2019.04.002.

AUTHOR CONTRIBUTIONS

P.N., H.N., Z.S., J.N.H., B.A., C. F., J. P., and S.C. designed the experiments. P.N., H.N., Z.S., Q.Z., Y.G., J.J.P., F.A., J.M.P., E.B., A.M., P.S., B.A., C.F., J.P., L.M.E., K.P., V.Y.B., and S.C. conducted experiments, collected data, and analyzed data. J.N.H. performed bioinformatics analysis. P.N., A.M., P.S., and S.C. wrote the manuscript. S.C. supported this study financially.

CONFLICTS OF INTEREST

The authors declare no competing interests.

ACKNOWLEDGMENTS

The authors are appreciative of the New York Medical College/Westchester Medical Center Translational Stem Cell Center for its support with confocal imaging. This study was supported by MH107884 (S.C.) and NYSTEM C32607GG (S.C.). Work by J.N.H. at the Harvard Chan Bioinformatics Core was supported by funding from the Harvard NeuroDiscovery Center.

REFERENCES

1. Wonders, C., and Anderson, S.A. (2005). Cortical interneurons and their origins. Neuroscientist *11*, 199–205.
2. Bandler, R.C., Mayer, C., and Fishell, G. (2017). Cortical interneuron specification: the juncture of genes, time and geometry. Curr. Opin. Neurobiol. *42*, 17–24.
3. Marín, O. (2012). Interneuron dysfunction in psychiatric disorders. Nat. Rev. Neurosci. *13*, 107–120.
4. Zhu, Q., Naegele, J.R., and Chung, S. (2018). Cortical GABAergic Interneuron/Progenitor Transplantation as a Novel Therapy for Intractable Epilepsy. Front. Cell. Neurosci. *12*, 167.
5. Takahashi, K., and Yamanaka, S. (2006). Induction of pluripotent stem cells from mouse embryonic and adult fibroblast cultures by defined factors. Cell *126*, 663–676.
6. Liu, Y., Weick, J.P., Liu, H., Krencik, R., Zhang, X., Ma, L., Zhou, G.M., Ayala, M., and Zhang, S.C. (2013). Medial ganglionic eminence-like cells derived from human embryonic stem cells correct learning and memory deficits. Nat. Biotechnol. *31*, 440–447.
7. Goldman, S.A. (2016). Stem and Progenitor Cell-Based Therapy of the Central Nervous System: Hopes, Hype, and Wishful Thinking. Cell Stem Cell *18*, 174–188.

8. Kikuchi, T., Morizane, A., Doi, D., Magotani, H., Onoe, H., Hayashi, T., Mizuma, H., Takara, S., Takahashi, R., Inoue, H., et al. (2017). Human iPS cell-derived dopaminergic neurons function in a primate Parkinson's disease model. Nature *548*, 592–596.

9. Rhee, Y.H., Ko, J.Y., Chang, M.Y., Yi, S.H., Kim, D., Kim, C.H., Shim, J.W., Jo, A.Y., Kim, B.W., Lee, H., et al. (2011). Protein-based human iPS cells efficiently generate functional dopamine neurons and can treat a rat model of Parkinson disease. J. Clin. Invest. *121*, 2326–2335.

10. Southwell, D.G., Nicholas, C.R., Basbaum, A.I., Stryker, M.P., Kriegstein, A.R., Rubenstein, J.L., and Alvarez-Buylla, A. (2014). Interneurons from embryonic development to cell-based therapy. Science *344*, 1240622.

11. Tabar, V., and Studer, L. (2014). Pluripotent stem cells in regenerative medicine: challenges and recent progress. Nat. Rev. Genet. *15*, 82–92.

12. Zhao, C., Wang, Q., and Temple, S. (2017). Stem cell therapies for retinal diseases: recapitulating development to replace degenerated cells. Development *144*, 1368–1381.

13. Bráz, J.M., Sharif-Naeini, R., Vogt, D., Kriegstein, A., Alvarez-Buylla, A., Rubenstein, J.L., and Basbaum, A.I. (2012). Forebrain GABAergic neuron precursors integrate into adult spinal cord and reduce injury-induced neuropathic pain. Neuron *74*, 663–675.

14. Cunningham, M., Cho, J.H., Leung, A., Savvidis, G., Ahn, S., Moon, M., Lee, P.K., Han, J.J., Azimi, N., Kim, K.S., et al. (2014). hPSC-derived maturing GABAergic interneurons ameliorate seizures and abnormal behavior in epileptic mice. Cell Stem Cell *15*, 559–573.

15. Donegan, J.J., Tyson, J.A., Branch, S.Y., Beckstead, M.J., Anderson, S.A., and Lodge, D.J. (2017). Stem cell-derived interneuron transplants as a treatment for schizophrenia: preclinical validation in a rodent model. Mol. Psychiatry *22*, 1492–1501.

16. Martínez-Cerdeño, V., Noctor, S.C., Espinosa, A., Ariza, J., Parker, P., Orasji, S., Daadi, M.M., Bankiewicz, K., Alvarez-Buylla, A., and Kriegstein, A.R. (2010). Embryonic MGE precursor cells grafted into adult rat striatum integrate and ameliorate motor symptoms in 6-OHDA-lesioned rats. Cell Stem Cell *6*, 238–250.

17. Maroof, A.M., Keros, S., Tyson, J.A., Ying, S.W., Ganat, Y.M., Merkle, F.T., Liu, B., Goulburn, A., Stanley, E.G., Elefanty, A.G., et al. (2013). Directed differentiation and functional maturation of cortical interneurons from human embryonic stem cells. Cell Stem Cell *12*, 559–572.

18. Kim, T.G., Yao, R., Monnell, T., Cho, J.H., Vasudevan, A., Koh, A., Peeyush, K.T., Moon, M., Datta, D., Bolshakov, V.Y., et al. (2014). Efficient specification of interneurons from human pluripotent stem cells by dorsoventral and rostrocaudal modulation. Stem Cells *32*, 1789–1804.

19. Nicholas, C.R., Chen, J., Tang, Y., Southwell, D.G., Chalmers, N., Vogt, D., Arnold, C.M., Chen, Y.J., Stanley, E.G., Elefanty, A.G., et al. (2013). Functional maturation of hPSC-derived forebrain interneurons requires an extended timeline and mimics human neural development. Cell Stem Cell *12*, 573–586.

20. Sun, A.X., Yuan, Q., Tan, S., Xiao, Y., Wang, D., Khoo, A.T., Sani, L., Tran, H.D., Kim, P., Chiew, Y.S., et al. (2016). Direct Induction and Functional Maturation of Forebrain GABAergic Neurons from Human Pluripotent Stem Cells. Cell Rep. *16*, 1942–1953.

21. Yang, N., Chanda, S., Marro, S., Ng, Y.H., Janas, J.A., Haag, D., Ang, C.E., Tang, Y., Flores, Q., Mall, M., et al. (2017). Generation of pure GABAergic neurons by transcription factor programming. Nat. Methods *14*, 621–628.

22. Colasante, G., Lignani, G., Rubio, A., Medrihan, L., Yekhlef, L., Sessa, A., Massimino, L., Giannelli, S.G., Sacchetti, S., Caiazzo, M., et al. (2015). Rapid Conversion of Fibroblasts into Functional Forebrain GABAergic Interneurons by Direct Genetic Reprogramming. Cell Stem Cell *17*, 719–734.

23. Hoffman, G.E., Hartley, B.J., Flaherty, E., Ladran, I., Gochman, P., Ruderfer, D.M., Stahl, E.A., Rapoport, J., Sklar, P., and Brennand, K.J. (2017). Transcriptional signatures of schizophrenia in hiPSC-derived NPCs and neurons are concordant with post-mortem adult brains. Nat. Commun. *8*, 2225.

24. Berkowitz, A.L., Miller, M.B., Mir, S.A., Cagney, D., Chavakula, V., Guleria, I., Aizer, A., Ligon, K.L., and Chi, J.H. (2016). Glioproliferative Lesion of the Spinal Cord as a Complication of "Stem-Cell Tourism". N. Engl. J. Med. *375*, 196–198.

25. Amariglio, N., Hirshberg, A., Scheithauer, B.W., Cohen, Y., Loewenthal, R., Trakhtenbrot, L., Paz, N., Koren-Michowitz, M., Waldman, D., Leider-Trejo, L., et al. (2009). Donor-derived brain tumor following neural stem cell transplantation in an ataxia telangiectasia patient. PLoS Med. *6*, e1000029.

26. Shao, Z., Noh, H., Bin Kim, W., Ni, P., Nguyen, C., Cote, S.E., Noyes, E., Zhao, J., Parsons, T., Park, J.M., et al. (2019). Dysregulated protocadherin-pathway activity as an intrinsic defect in induced pluripotent stem cell-derived cortical interneurons from subjects with schizophrenia. Nat. Neurosci. *22*, 229–242.

27. Saxena, A., Wagatsuma, A., Noro, Y., Kuji, T., Asaka-Oba, A., Watahiki, A., Gurnot, C., Fagiolini, M., Hensch, T.K., and Carninci, P. (2012). Trehalose-enhanced isolation of neuronal sub-types from adult mouse brain. Biotechniques *52*, 381–385.

28. Faux, C., Rakic, S., Andrews, W., Yanagawa, Y., Obata, K., and Parnavelas, J.G. (2010). Differential gene expression in migrating cortical interneurons during mouse forebrain development. J. Comp. Neurol. *518*, 1232–1248.

29. Okaty, B.W., Miller, M.N., Sugino, K., Hempel, C.M., and Nelson, S.B. (2009). Transcriptional and electrophysiological maturation of neocortical fast-spiking GABAergic interneurons. J. Neurosci. *29*, 7040–7052.

30. Wonders, C.P., and Anderson, S.A. (2006). The origin and specification of cortical interneurons. Nat. Rev. Neurosci. *7*, 687–696.

31. Buchanan, S.S., Gross, S.A., Acker, J.P., Toner, M., Carpenter, J.F., and Pyatt, D.W. (2004). Cryopreservation of stem cells using trehalose: evaluation of the method using a human hematopoietic cell line. Stem Cells Dev. *13*, 295–305.

32. Lee, Y.A., Kim, Y.H., Kim, B.J., Kim, B.G., Kim, K.J., Auh, J.H., Schmidt, J.A., and Ryu, B.Y. (2013). Cryopreservation in trehalose preserves functional capacity of murine spermatogonial stem cells. PLoS ONE *8*, e54889.

33. Thomsen, M.S., Hansen, H.H., Timmerman, D.B., and Mikkelsen, J.D. (2010). Cognitive improvement by activation of alpha7 nicotinic acetylcholine receptors: from animal models to human pathophysiology. Curr. Pharm. Des. *16*, 323–343.

34. Franco, R., and Cedazo-Minguez, A. (2014). Successful therapies for Alzheimer's disease: why so many in animal models and none in humans? Front. Pharmacol. *5*, 146.

35. Xiang, Y., Tanaka, Y., Patterson, B., Kang, Y.J., Govindaiah, G., Roselaar, N., Cakir, B., Kim, K.Y., Lombroso, A.P., Hwang, S.M., et al. (2017). Fusion of Regionally Specified hPSC-Derived Organoids Models Human Brain Development and Interneuron Migration. Cell Stem Cell *21*, 383–398.e7.

36. Bagley, J.A., Reumann, D., Bian, S., Lévi-Strauss, J., and Knoblich, J.A. (2017). Fused cerebral organoids model interactions between brain regions. Nat. Methods *14*, 743–751.

37. Monzel, A.S., Smits, L.M., Hemmer, K., Hachi, S., Moreno, E.L., van Wuellen, T., Jarazo, J., Walter, J., Brüggemann, I., Boussaad, I., et al. (2017). Derivation of Human Midbrain-Specific Organoids from Neuroepithelial Stem Cells. Stem Cell Reports *8*, 1144–1154.

38. Ogawa, J., Pao, G.M., Shokhirev, M.N., and Verma, I.M. (2018). Glioblastoma Model Using Human Cerebral Organoids. Cell Rep. *23*, 1220–1229.

39. Lamas, N.J., Johnson-Kerner, B., Roybon, L., Kim, Y.A., Garcia-Diaz, A., Wichterle, H., and Henderson, C.E. (2014). Neurotrophic requirements of human motor neurons defined using amplified and purified stem cell-derived cultures. PLoS ONE *9*, e110324.

40. Jacobs, J.S., and Miller, M.W. (2000). Cell cycle kinetics and immunohistochemical characterization of dissociated fetal neocortical cultures: evidence that differentiated neurons have mitotic capacity. Brain Res. Dev. Brain Res. *122*, 67–80.

41. Kemp, P.J., Rushton, D.J., Yarova, P.L., Schnell, C., Geater, C., Hancock, J.M., Wieland, A., Hughes, A., Badder, L., Cope, E., et al. (2016). Improving and accelerating the differentiation and functional maturation of human stem cell-derived neurons: role of extracellular calcium and GABA. J. Physiol. *594*, 6583–6594.

42. Wang, J., Ye, Z., Zheng, S., Chen, L., Wan, Y., Deng, Y., and Yang, R. (2016). Lingo-1 shRNA and Notch signaling inhibitor DAPT promote differentiation of neural stem/progenitor cells into neurons. Brain Res. *1634*, 34–44.

43. Yoon, K., and Gaiano, N. (2005). Notch signaling in the mammalian central nervous system: insights from mouse mutants. Nat. Neurosci. *8*, 709–715.

44. Louvi, A., and Artavanis-Tsakonas, S. (2006). Notch signalling in vertebrate neural development. Nat. Rev. Neurosci. *7*, 93–102.

45. Schizophrenia Working Group of the Psychiatric Genomics Consortium (2014). Biological insights from 108 schizophrenia-associated genetic loci. Nature *511*, 421–427.

46. Shao, Z., Noh, H., Bin Kim, W., Ni, P., Nguyen, C., Cote, S.E., Noyes, E., Zhao, J., Parsons, T., and Park, J.M. (2019). Dysregulated protocadherin-pathway activity as an intrinsic defect in induced pluripotent stem cell-derived cortical interneurons from subjects with schizophrenia. Nat Neurosci *22*, 229–242.

47. Carvalho, B.S., and Irizarry, R.A. (2010). A framework for oligonucleotide microarray preprocessing. Bioinformatics *26*, 2363–2367.

48. Gautier, L., Cope, L., Bolstad, B.M., and Irizarry, R.A. (2004). affy–analysis of Affymetrix GeneChip data at the probe level. Bioinformatics *20*, 307–315.

49. Kauffmann, A., Gentleman, R., and Huber, W. (2009). arrayQualityMetrics–a bioconductor package for quality assessment of microarray data. Bioinformatics *25*, 415–416.

50. Irizarry, R.A., Hobbs, B., Collin, F., Beazer-Barclay, Y.D., Antonellis, K.J., Scherf, U., and Speed, T.P. (2003). Exploration, normalization, and summaries of high density oligonucleotide array probe level data. Biostatistics *4*, 249–264.

51. Taminau, J., Meganck, S., Lazar, C., Steenhoff, D., Coletta, A., Molter, C., Duque, R., de Schaetzen, V., Weiss Solís, D.Y., Bersini, H., and Nowé, A. (2012). Unlocking the potential of publicly available microarray data using inSilicoDb and inSilicoMerging R/Bioconductor packages. BMC Bioinformatics *13*, 335.

52. Hong, S., Hwang, D.Y., Yoon, S., Isacson, O., Ramezani, A., Hawley, R.G., and Kim, K.S. (2007). Functional analysis of various promoters in lentiviral vectors at different stages of in vitro differentiation of mouse embryonic stem cells. Mol. Ther. *15*, 1630–1639.